Brain Stimulation 13 (2020) 819–831

Contents lists available at ScienceDirect

Brain Stimulation

journal homepage: http://www.journals.elsevier.com/brain-stimulation

Cortico-cortical connectivity between the superior and inferior parietal lobules and the motor cortex assessed by intraoperative dual cortical stimulation

Luigi Cattaneo [a, c, *], Davide Giampiccolo [a, b], Pietro Meneghelli [b], Vincenzo Tramontano [b], Francesco Sala [a, b]

[a] Department of Neuroscience, Biomedicine and Movement, Section of Physiology and Psychology, University of Verona, Verona, Italy
[b] Neurosurgery Unit, Neuroscience Department, Azienda Ospedaliera Universitaria Integrata, Verona, Italy
[c] Center for Mind/Brain Sciences (CIMeC), University of Trento, Trento, Italy

ARTICLE INFO

Article history:
Received 29 August 2019
Received in revised form
7 February 2020
Accepted 18 February 2020
Available online 21 February 2020

ABSTRACT

Background: The function of the primate's posterior parietal cortex (PPC) in sensorimotor transformations is well-established, though in humans its complexity is still challenging. Well-established models indicate that the posterior parietal cortex influences motor output indirectly, by means of connections to the premotor cortex, which in turn is directly connected to the motor cortex.
Objective: The possibility that the PPC could be at the origin of direct afferents to M1 has been suggested in humans but has never been confirmed directly. We aim to do so in the present study by using the novel technique of paired intraoperative cortical stimulation.
Methods: In the present cross-sectional study, we assessed during intraoperative monitoring of the corticospinal tract in brain tumour patients the existence of short-latency effects of parietal stimulation on corticospinal excitability to the upper limb. MEPs were evoked by test stimuli over the motor cortex, which were preceded in some trials by conditioning stimuli on the PPC.
Results: We identified two active cortical loci. One in the inferior parietal lobule exerted short-latency excitatory effects and one in the superior parietal lobule that drove short-latency inhibitory effects on cortical motor output. All active foci were distributed in the rostral portion of the PPC and on the postcentral sulcus.
Conclusions: For the first time in humans, the present data show direct evidence in favour of a distributed system of connections from the posterior parietal cortex to the ipsilateral primary motor cortex. In addition, we show that dual cortical stimulation is a novel and efficient technique to investigate intraoperative brain connectivity in the anaesthetized patient.

Introduction

The last 40 years have witnessed a radical change in our view of the parietal cortex [1]. The posterior parietal cortex, once labelled as "associative cortex" is now well-known for receiving multimodal sensory information and integrating it into a praxic, behaviourally-committed representation of the world around us. Solid evidence in the field of neuropsychology, neuroimaging and neurostimulation indicates that the posterior parietal cortex is necessary for goal-directed behaviour [2–5]. Symptoms frequently caused by lesions of the parietal lobe include deficits in sensorimotor processes, such as optic ataxia [6] or apraxia [7]. Direct stimulation of the human parietal cortex has been shown to produce movements in all body segments [8,9]. Current evidence indicates that the human superior parietal lobule is involved in sensorimotor transformation for spatially-oriented, proximal movements as in reaching out for an object (for a review see Refs. [10–12]), but also involved in neural control of distal movements such as grasping [13,14]. Visual features of objects, used to guide distal, object-directed movements are represented in humans in the anterior intraparietal region [2,15–21]. The role of the inferior parietal lobule in movement is less clear. Grasping-related activity in the anterior intraparietal

* Corresponding author. Center for Mind/Brain Sciences (CIMeC), University of Trento, Via delle Regole 101, 38123, Trento, Italy.
E-mail address: luigi.cattaneo@unitn.it (L. Cattaneo).

https://doi.org/10.1016/j.brs.2020.02.023

region is found along the descending part of the precentral sulcus, up to the parietal operculum with some specialization for tool use of the more ventral areas [2]. More ventrally, the parietal opercular region is also thought to be a site of sensorimotor integration, mainly in the somatosensory modality [22–24]. Summing up, converging data from functional neuroimaging and lesion mapping in humans indicate an extended region ranging from the superior parietal lobule (Brodmann's areas 5 and 7), to the whole intraparietal region, up to the parietal operculum and supramarginal gyrus (Brodmann's area 40) are involved in sensorimotor processes and specialized in distinct functional aspects.

How does the motor cortex use motor-relevant information from the posterior parietal cortex? The influence of the parietal cortex on motor output is generally considered to be indirect. According to influential models, based on monkey anatomy, the parietal cortex modulates corticospinal activity in an indirect way, through the premotor cortex [25–28]. However, even anatomical data in monkeys are controversial in this respect. The existence of direct, monosynaptic connections from the posterior parietal cortex to the upper limb representation of the primary motor cortex has been demonstrated by several independent works [29–31]. Such data offer the anatomical bases for a possible direct pathway by which the posterior parietal cortex might control directly corticospinal output. In addition to this, it has been recently shown that the posterior parietal cortex of macaques has a direct access to spinal motor neurons by means of corticospinal axons [32]. In humans, several recent lines of evidence have suggested that the posterior parietal cortex might have a more direct influence on motor output. Non-invasive brain stimulation, i.e. transcranial magnetic stimulation (TMS) suggests that the parietal cortex could give origin to direct cortico-cortical connections to the primary motor cortex (M1) [33–39], involved in skilled upper limb movements. Summing up, there is ample evidence in both nonhuman and human primates to support the possibility that the parietal lobe could modulate corticospinal output also directly through M1, besides the well-established indirect pathway through a relay in the premotor cortex (see Refs. [40,41] for a review of parieto-M1 interaction models). The active role of the posterior parietal cortex in producing movements is being currently re-evaluated as a potential source of "pre-motor" afferents to the premotor cortex, where pre-motor is used here in a functional sense rather than anatomical. Imaging data provided indirect evidence of posterior parietal-motor anatomical and functional connectivity [35,42,43]. However, direct evidence in favour of direct connections between the parietal and the motor cortex in humans are lacking.

We aim to fill this gap in current knowledge with the present work in which we tested cortico-cortical connectivity by means of intra-operative direct cortical stimulation (DCS) with a dual-pulse paradigm similar to that employed with dual-coil TMS [40]. Supra-threshold test stimuli were delivered to M1 and the resulting motor evoked potentials (MEPs) were systematically recorded form distal upper limb muscles, and in some cases from facial and lower limb muscles. In some trials a conditioning stimulus was delivered to different regions of the parietal cortex at variable inter-stimulus intervals (ISIs) ranging from 4 ms to 16 ms. In some other trials, only conditioning stimuli were delivered. The conditioning stimulus itself does not activate the corticospinal motor pathways, as witnessed by the systematic absence of MEPs in such trials. The modulation of motor output by conditioning stimuli is generally considered as evidence of cortico-cortical functional connectivity between the target of conditioning stimuli and the motor cortex. It is important to note that a necessary pre-requisite for the realization of dual-stimulation paradigms is that the corticospinal tract must be activated *trans*-synaptically by the test stimuli, because direct axonal stimulation of corticospinal axons produces MEPs that arise downstream of the putative site of interaction between the conditioning and the test stimuli. In this respect, the information currently available indicates that direct cortical stimulation (DCS) is effective also under general anaesthesia in exciting cortical output *trans*-synaptically, also at low stimulation intensities [44–47]. Invasive intra-operative monitoring (IONM) in neurosurgery therefore offers the unique opportunity to assess cortico-cortical connectivity *in vivo*, with extraordinary spatial resolution and anatomical precision.

We know from previous literature that a vast portion of the parietal cortex is involved during hand movements, comprising the whole anterior part of the convexity of the parietal lobes, ranging from Brodmann's areas 5 and 7 to Brodmann's area 40 and the parietal opercular region. A recent meta-analysis of more than 2000 fMRI scans obtained during voluntary movements confirmed that the whole rostral portion of the PPC is active and possibly plays some role when the subject is actually moving [48]. Therefore, in the present work we adopted an exploratory strategy, trying to sample in different patients, different parts of the parietal cortex, i.e. the rostral half of the superior parietal lobule and of the inferior parietal lobule (Fig. 1C). We aimed to obtain a partially overlapping, but even sampling of the parietal regions of interest. It is worth noting that the intraparietal sulcus, a region of great interest for hand movements [2] is excluded from the exploration because surface cortical stimulation does not reach the depth of the sulcus. Indeed, the results of the present work indicated a diffuse field of parietal spots exerting short-latency modulation of corticospinal output in the range of 4–16 ms of inter-stimulus intervals, distributed along the post-central sulcus. Such active spots showed higher density in two large clusters in the superior inferior parietal lobules. The present study does not have any potential significance in terms of brain-behavioural relations because it is entirely conducted in anaesthetized subjects, it merely points at the existence of functional circuitry, the significance of which is yet to be determined.

Materials and methods

Patients

The study proposal is in accordance with ethical standards of the Declaration of Helsinki. All stimulations and recordings were performed in the context of clinical intraoperative neurophysiological monitoring (IONM) to which all patients gave informed consent. Patients scheduled for tumour removal in the vicinity of the parietal cortex were screened for enrolment. The inclusion criteria were: (1) brain tumour necessitating intraoperative neurophysiological monitoring (2) over 18 years of age. Exclusion criteria were (1) extended cortico-subcortical damage to the parietal lobe (2) voluntary decision of the patient not to be included in the cohort. Seventeen patients (age 39–79; 10M-7F; 17 right-handed) were included in this study, recruited from the Verona University Hospital in the 2015–2019 interval. Eight patients had right-sided lesions and 9 had left-sided lesion. Patient's characteristics are presented in Table 1.

Stereotaxic neuronavigation and electrode placement

MRI scans of each patient's brain were acquired before surgery on a 3T scanner with an eight-channel head coil (Signa *3T*, *General Electric* Healthcare, Milwaukee, USA). T1-weighted 3D MPRAGE images were acquired using the following parameters (echo train length: 1, TE: 2.67 ms, TR: 2.000, matrix size: 256 × 246, slice thickness: 1 mm). T2-weighted, FLAIR images were also acquired (TR 6000 ms, TE 150 ms, TI 2000 ms). The reconstruction of the

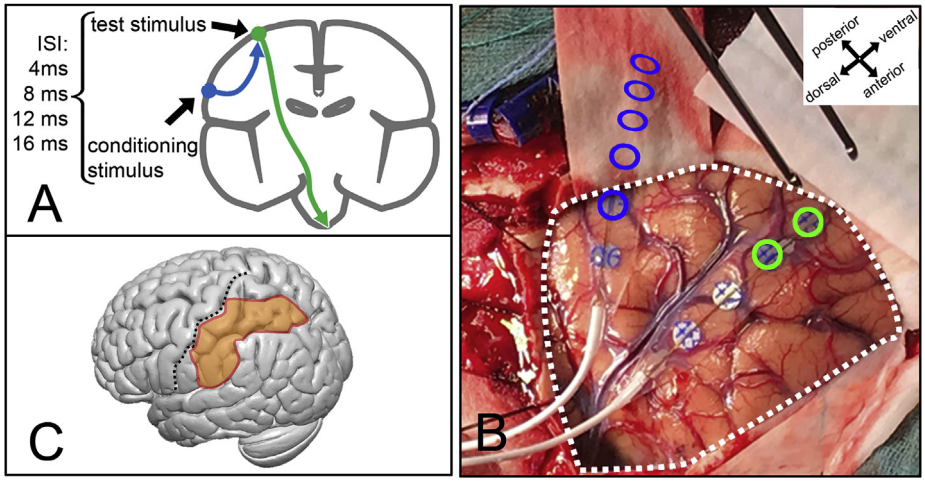

Fig. 1. A - schematic representation of the dual strip protocol. Test stimuli are delivered to the motor cortex and produce a measurable motor evoked potential via the corticospinal tract (green arrow). In some trials the test stimulus is preceded by a conditioning stimulus, which alone cannot activate the corticospinal tract, applied to the parietal cortex (blue arrow). The inter-stimulus interval (ISI) ranges between 4 and 16 ms. **B -** Actual surgical scenario (patient #4). The dashed white line represents the borders of the craniotomy. The two stimulation strips are shown. The test stimulus dipole is indicated with the two green circles and is used to activate the corticospinal tract. The conditioning strip is placed over the parietal lobe. The dipoles used for conditioning stimuli are indicated with blue circles. Note that the electrode strip is inserted under the dura, therefore the electrode position extends well beyond the craniotomy. **C** – parietal region that is involved in voluntary movements (redrawn from Ref. [48]) and that was assumed as target for conditioning electrode position. (For interpretation of the references to colour in this figure legend, the reader is referred to the Web version of this article.)

individual cortical surface was performed using Brainsuite (Brainsuite, UCLA Brain Mapping Center, San Francisco, USA) [49]. For a clearer intraoperative visualization of sulcal anatomy, a skull stripped T1 using a non-uniformity correction or a FLAIR image was added to the 3D visualization of the Neuronavigation system (Stealth Station 7, Medtronic, Minneapolis, USA). Correspondence of 3D reconstruction and individual patient's sulcal anatomy was then performed using the Neuronavigation pointer. Brain anatomy was systematically analysed prior to surgery so that main sulcal patterns of the postcentral and parietal region could be readily identified during actual surgery. The stimulating strip was placed parallel to the central sulcus, similarly to the montage used for studies of intra-operative motor evoked potentials, after identification of the central sulcus by phase reversal [50]. Placement of the conditioning electrode strip was roughly planned a priori but was systematically reprogrammed when in presence of contingent surgical conditions preventing the placement of the strip in the desired position, such as presence of large vessels or space requirements by the ongoing surgical procedures.

Anaesthesia and conventional IONM

The anaesthesia protocol applied was Total Intravenous Anaesthesia (TIVA). More precisely, a continuous infusion of Propofol (100–150 μg/kg/min) and Fentanyl (1 μg/kg/min) was used, avoiding bolus. Short acting relaxants were administered for intubation purpose only and then avoided. Halogenated anaesthetic agents were never used. Since all patients were candidates for

Table 1
Demographic information on the group of patients.

Patient #, age, dexterity, sex.	Symptoms at presentation	Anatomical location of the lesion	Characterization of the neoplastic lesion
#1–60 y-o right-handed female	Apraxia, gait disturbances, dysesthesia and weakness on the right side	Right post-central,inhomogeneous lesion	Glioma IV (WHO 2016, IDH-WT, MGMT+)
#2–71 y-o, right-handed male	Gait ataxia, dysarthria	Right frontal homogeneous lesion	Meningioma I (WHO 2016, A)
#3–62 y-o right-handed female	Left facial palsy of central type	right post-Rolandic inhomogeneous lesion	Glioma IV (WHO 2016, IDH- WT, MGMT+)
#4–71 y-o, right-handed male	dysesthesia and weakness of the right arm and face; mild language deficits	left anterior intraparietal inhomogeneous lesion	Metastatic melanoma (VBRAF+)
#5–62 y-o right- handed female	Leg weakness	Left pre-Rolandic inhomogeneous lesion	Metastatic lung adenocarcinoma (PDL-2 +)
#6–62 y-o right handed female	Headache	Left frontal parasagittal homogenous lesion	Meningioma I (WHO 2016, A)
#7–74 y-o, right-handed male	Right leg weakness	Left frontal parasagittal homogenous lesion	Meningioma II (WHO 2016, A)
#8–75 y-o right- handed female	Generalized seizures	Right parieto-temporal inhomogeneous lesion	Glioma IV (WHO 2016, IDH- WT, MGMT-)
#9–60 y-o right- handed female	Mood change	Right pre-Rolandic inhomogeneous lesion	Metastatic lung adenocarcinoma (PDL-1 +)
#10–67 y-o, right-handed male	Dizziness, gait ataxia	Right parieto-temporal inhomogeneous lesion	Glioma IV (WHO 2016, IDH- WT, MGMT+)
#11–77 y-o, right-handed male	Focal seizures, dizziness, left homonymous hemianopia	Right parieto-temporal inhomogeneous lesion	Glioma IV (WHO 2016, IDH- WT, MGMT+)
#12–79 y-o right handed male	Dizziness	Right Rolandic homogenous lesion	Meningioma I (WHO 2016, A-B)
#13–74 y-o, right-handed male	Enhancing lesion on follow up (redo)	Left superior frontal inhomogeneous lesion	Glioma IV (WHO 2016, IDH-1, MGMT+)
#14–32 y-o, right-handed male	Focal seizures	Right superior temporal homogenous lesion	Ganglioglioma I (WHO 2016, A-B)
#15–37 y-o, right-handed male	Focal seizures, mild language deficits (Redo)	Left temporal inhomogenous lesion	Glioma IV (WHO 2016, IDH- WT, MGMT-)
#16–49 y-o right-handed female	Generalized seizures (Redo)	Left temporo-polar inhomogeneous lesion	Glioma IV (WHO 2016, IDH- WT, MGMT+)
#17–52 y-o, right-handed male	Right side weakness, mild language deficits	Left temporo-polar inhomogeneous lesion	Glioma IV (WHO 2016, IDH- WT, MGMT+)

IONM of the corticospinal tract, standard neurophysiological monitoring and mapping was performed. This involved simultaneous acquisition of continuous electroencephalography (EEG), electrocorticography (ECoG), recording of free-running electromyographic (EMG) activity by means of a commercial intraoperatory poligraphy system (ISIS-IOM, Inomed Medizintechnik GmbH, Emmendingen, Germany). Muscle MEPs were initially elicited by Transcranial Electrical Stimulation (TES) via corkscrew-like electrodes (Ambu® Neuroline Corkscrew, Ambu, Copenhagen, Denmark) from the scalp. Short trains of 5 square-wave stimuli of 0.5 ms duration, and interstimulus interval (ISI) of 4 ms were applied at a repetition rate up to 2 Hz through electrodes placed at C1 and C2 scalp sites, according to the 10/20 EEG system. Cortical and subcortical stimulation were performed using a monopolar probe (45 mm, angled 30°, Inomed Medizintechnik GmbH, Emmendingen, Germany) referenced to Fz. Stimulation parameters were as follows: a short train of five pulses, pulse duration 0.5 ms; interstimulus interval (ISI) 2 ms at 1 Hz repetition rate. Cortical stimulation was anodal while subcortical stimulation was cathodal. Once the dura was opened, MEP monitoring was performed using a 6-contacts strip electrode with diameter 2.5 mm, space 10 mm, contact strips: 0.7 mm thin, 10 mm width (Inomed Medizintechnik GmbH, Emmendingen, Germany). EMG recordings were performed in a belly-tendon montage, by means of subcutaneous needle monopolar electrodes (Ambu® Neuroline Subdermal, Ambu, Copenhagen, Denmark). The *orbicularis oris*, the *abductor pollicis brevis* (APB), the *biceps*, the *abductor hallucis* and the *tibialis anterior* muscles contralateral to the stimulated hemisphere were recorded.

Dual strip stimulation

Direct electrical cortical stimulation was applied to the precentral gyrus (test stimuli) via a 6-contacts strip electrode and to the parietal cortex by means of a 6-contacts or an 8-contacts strip electrode (Fig. 1 shows a schematic of the dual strip protocol and an example of surgical scenario). Test stimuli were delivered with trains of the minimal duration required to elicit a stable MEP in the ABP. This results in test stimulation with one single stimulus in 1 patient, with 2 stimuli in 12 patients and with 3 stimuli in 3 patients. Intensity of test stimulation was set to obtain a MEP from the thenar muscle of around 500 μV peak-peak amplitude. Mean stimulus intensity in the population was 21.9 mA (SD = 6.3 mA), ranging from 15 to 35 mA. Stimulation of the PPC alone does not produce any measurable output. We used therefore stimulation intensity that was verified to activate corticofugal pathways in the individual patient. To standardize timing precision between the conditioning and the test stimuli between all patients, the conditioning stimuli were always delivered in a short train of 2 stimuli at 250 Hz and of 0.5 ms duration at the same intensity as that of test stimuli. Prior to all experimental stimulations we acquired blocks of conditioning stimuli alone, verifying that no MEP could be observed from test stimulation.

The ISI was considered as the interval between the last stimulus of the conditioning train and the last pulse of the test train. The ISIs of 4 ms, 8 ms, 12 ms and 16 ms were explored in separate blocks for each of the test-stimulus electrodes. The choice of ISIs was made by comparison with the previous literature. Dual cortical stimuli between the premotor cortex and M1 in macaques (the two stimulation sites are around 15 mm apart) have shown to interact at ISIs of 3 ms [51]. In humans, TMS data indicates interactions in the 3–15 ms range [33,36,40,52]. Both human and monkey data have been acquired in the un-anaesthetized subject. Based on monkey findings we would have predicted that interaction between two cortical regions 30–60 mm apart would be between 6 and 12 ms; conversely, based on human data, we would expected interactions to start around 4 ms, hence our choice of ISIs. Every block contained at least 15 repetitions of the same dual stimulation. Dual-stimulation blocks were alternated with blocks with only test-stimuli so that the unconditioned MEP amplitude was monitored throughout the recording session. The timing of dual stimuli was managed entirely by the commercially available ISIS-IOM system (Inomed Medizintechnik GmbH, Emmendingen, Germany) by means of the “facilitation” function, that allows independent electrical stimulation through two separate output channels. Not all ISIs were explored in every subject due to time constraints.

Data analysis

Pre-processing required the data to be exported in digital format and analysed with the MATLAB software. A FIR filter was applied with a pass-band of 50–2000 Hz and a transition gap of 30 Hz. MEP signal is commonly high-pass filtered at much lower frequencies, but in the present case, the measurement of MEP areas prompted us to eliminate any low-frequency noise that could add up to the waveform’s area. The filtered EMG was rectified and the duration of the MEP was determined individually, and the corresponding area of the EMG recording was extracted. In this way each trial was characterized by a single number, i.e. the MEP area. MEP areas are known to covary linearly with MEP amplitudes, therefore the two measures are equivalent [53,54]. We chose to measure MEP areas instead of peak-peak amplitudes, because in several patients the MEPs had complex, polyphasic waveforms, and in such cases MEPs areas are a more robust measure than amplitudes [55]. We then proceeded to normalizing conditioned MEPs to test MEPs. However, MEPs to test stimuli alone are not stable throughout the surgical procedure because of strip movements. To correct for such variability, we normalized blocks of conditioned MEPs only to a sliding window of the blocks of test stimuli adjacent to each conditioned block. This was done by dividing the single conditioned MEP areas by the median of the test MEP areas in adjacent blocks. For example, in the following sequence: [test block 1] – [conditioned block 1] – [test block 2] – [conditioned block 2] – [test block 3] – [conditioned block 3] – [test block 4] – [conditioned block 4] - [test block 5], each conditioned MEP in conditioned block 1 was normalized to the median of the MEPs of test blocks 1 and 2. The MEPs from conditioned block 2 were normalized to the median of MEPs from test blocks 2 and 3. The resulting normalized conditioned MEP areas (normMEP) were used as main experimental variable. The main analysis was carried out in single patients, comparing normalized conditioned MEP areas from test stimuli by means of independent-samples t-tests. This test informs us whether, in single subjects, the trials in a given conditioned set are different from those in the test set and the direction of the change (excitation or inhibition). Significance threshold was corrected to account for the repeated comparisons. Analysis were performed therefore on single subjects, using a univariate approach. The results of single t-tests were therefore corrected for multiple comparisons in each participant. For example, patient #1 was tested on 20 cortical spots and therefore critical p-value was set to $p = 0.05/20$ i.e. $p = 0.0025$. Qualitative assessment of the effects of conditioning stimuli at the population level was performed by plotting on a standardized surface map of the parietal cortex the sites of conditioning stimulation of all participants, indicating electrodes that had a significant effect on test stimuli in single participants. To this purpose, we used the frameless stereotaxic neuronavigation system to pinpoint on individual brain anatomies the real position of strip electrodes and the trajectory of strips that were not readily visible because in the subdural space.

In order to standardize and describe individual electrode positions at the population level, we performed a normalization of the

Table 2
MNI coordinates of each electrode in the parietal cortex (the coordinates refer to the cathode of the stimulating dipole). The last column indicates the Euclidean distance in mm from teach electrode to the corresponding motor cortex electrode that delivered the test stimulus.

patient #	conditioning stimulus cathode	MNI coordinates			euclidean distance to motor cortex (mm)
		x	y	z	
1	P1	51	−59	53	47
	P2	51	−50	57	38
	P3	51	−41	60	29
	P4	51	−32	61	21
	P5	51	−24	63	14
2	P1	52	−30	58	21
	P2	48	−38	62	25
	P3	43	−43	67	28
	P4	36	−49	69	34
	P5	30	−52	73	39
3	P1	42	−35	63	20
	P2	30	−41	67	28
	P3	23	−45	72	35
4	P1	−37	−75	49	63
	P2	−38	−68	55	54
	P3	−37	−61	60	47
	P4	−41	−52	63	37
5	P1	−33	−67	55	54
	P2	−38	−58	57	44
	P3	−43	−49	62	34
	P4	−47	−38	63	24
6	P1	−54	−36	53	28
	P2	−57	−44	50	37
	P3	−55	−51	46	44
	P4	−54	−59	41	53
7	P1	−34	−45	75	32
	P2	−41	−43	68	28
	P3	−48	−43	61	29
	P4	−57	−39	56	31
8	P1	56	−36	60	27
	P2	60	−31	52	29
	P3	63	−27	43	35
	P4	65	−24	34	42
	P5	66	−21	25	49
9	P1	−65	0	31	46
	P2	−68	−11	30	46
	P3	−69	−21	30	47
10	P1	44	−27	62	13
	P2	50	−32	60	20
	P3	55	−38	57	29
	P4	60	−31	53	29
	P5	63	−24	48	30
11	P1	−64	−25	35	41
	P2	−60	−24	42	33
	P3	−56	−23	49	25
	P4	−51	−20	55	16
	P5	−44	−17	60	8
12	P1	54	−22	56	18
	P2	59	−27	50	28
	P3	63	−32	43	37
	P4	65	−36	35	45
13	P1	−45	−32	67	17
	P2	−41	−24	69	9
	P3	−36	−17	74	9
14	P1	57	−56	48	48
	P2	62	−51	41	49
	P3	67	−45	34	52
	P4	70	−38	28	54
	P5	70	−30	23	55
15	P1	−61	−49	31	53
	P2	−64	−43	23	57
	P3	−68	−35	16	61
	P4	−72	−29	8	68
	P5	−76	−22	1	75
16	P1	−67	24	16	69
	P2	−68	32	23	70
	P3	−67	40	30	71
	P4	−66	47	36	74
	P5	−65	55	43	78
17	P1	−53	−64	45	55
	P2	−46	−67	53	54
	P3	−37	−72	56	58
	P4	−27	−73	57	60
	P5	−19	−77	60	66

MRI with respective stimulation points to a MNI template. To do so we performed an enantiomeric coregistration or the individual MRI from the native space to the MNI using SPM (Friston et al., 1995) by masking the lesions to allow for the optimal coregistration. Stimulation points, which were all acquired intraoperatively using the neuronavigation, were normalized as well using the transformation matrix of each individual native space. As the minimal distance between two contacts of a strip electrode is 5 mm, a spherical ROI with diameter of 5 mm was used for every stimulation point. Individual electrode coordinates in MNI space are numbered in Table 2, together with their Euclidean distance from the motor cortex electrode. The single electrode coordinates were mapped onto a standard MNI template using MRIcroGL and the Surfice software for 3D rendering. It should be noted that the parietal region shows a considerable inter-individual variability [56], therefore relying on the standardized MNI transformed coordinates may produce slight inaccuracies in localizing the position of single spots with respect to major anatomical landmarks such as the intraparietal sulcus at the single-subject level. Nevertheless, this procedure allows for robust description of the data at the population level. Fig. 2 indicates individual brain anatomies of the 16 patients together with the conditioning strip electrodes and Fig. 4 Indicates the population data in the standardized MNI space. In 4 patients, also diffusion tensor imaging (DTI) scans were acquired for the purpose of surgical planning. In this very limited subset of patients we explored post-hoc the existence of tractographic streamlines connecting the spots of conditioning stimulation with the precentral gyrus. Results are illustrated in Supplementary materials.

The spatial distribution and clustering of the electrode positions was analysed by first extracting the principal components (PC) of the 3D distribution of the population of electrodes and then by performing a multi-dimensional test for comparing population means, i.e. Hotelling's T2 test, which is a multi-dimensional generalization of the *t*-test [57], to compare the distribution of inhibitory spots versus that of facilitatory spots.

The full set of MEP data is available at the Open Science Framework repository and is publicly accessible at the address: https://osf.io/dhcmk/

Results

In all participants it was possible to stimulate at least one conditioning spot, with a variable number of 3–6. Fig. 2 shows each patient's anatomy together with lesion location and electrode placement. For the sake of clarity, participants have been numbered according to the presence of excitatory effect, inhibitory effects or no effect. Fig. 3 shows 2 representative examples of facilitatory and inhibitory effects. We observed in most subjects a significant modulation of MEPs by conditioning stimuli in one specific electrode, at specific timings. The map of effective electrodes and the polarity of the effect are represented on a standardized MNI template in Fig. 4, left panel. Individual results are reported in Fig. 5 and in Table 3. We observed both inhibitory and excitatory effects of conditioning stimuli at different ISIs. The systematic between-

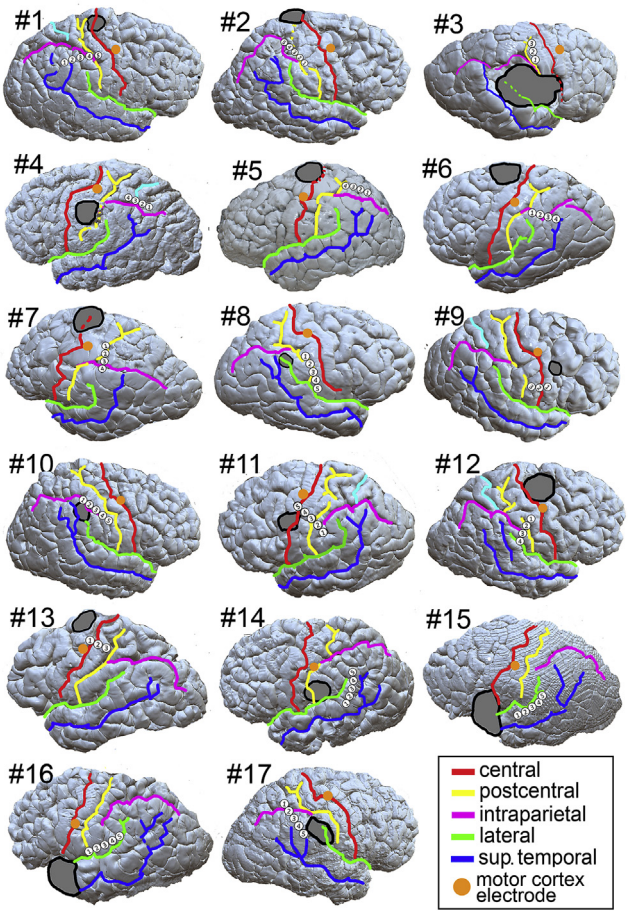

Fig. 2. Rendering of the individual brains (only the stimulated hemisphere is shown. The projection of the lesion on the surface is indicated with the grey shape. Main cortical sulci are indicated with a colour code as indicated in the legend. The orange spot indicates the point of corticospinal stimulation (test stimulus). The white numbered circles indicate the position of the cathode of conditioning stimulation. (note that conditioning stimuli have been delivered in bipolar modality). (For interpretation of the references to colour in this figure legend, the reader is referred to the Web version of this article.)

subject variations inherent in the mapping technique were reflected in the variability of the ISIs at which conditioning stimuli exerted a significant effect on corticospinal excitability which ranged from 4 ms to 16 ms. 6 participants showed only inhibitory effects, 3 showed mixed effects, 4 showed faciliatory effects and 4 did not show any effect of conditioning stimuli on corticospinal excitability.

Each patient was stimulated with conditioning stimuli in 2–5 pairs of stimulating electrodes (Fig. 2 indicates the cathode of the bipolar stimulation montages). Active spots were localized all along a rostral region of the PPC immediately posterior to the post-central sulcus (Fig. 4). In addition, in the few participants in which the conditioning stimulus strip reached the central sulcus, we observed a small cluster of active spots corresponding to the hand motor cortex. We excluded the spots on or frontal to the central sulcus (electrode P5 of patient 1, electrode P5 of patient 11 and electrodes P2 and P3 of patient 13). We did not observe significant effects from stimulation of the post-central gyrus at the ISIs adopted here. The polarity of the effect was spatially organized. We observed inhibitory effects of conditioning stimuli applied to the superior parietal lobule and the anterior intraparietal region. We found excitatory effects from conditioning stimuli applied to the inferior parietal lobule. Most patients showed only facilitatory or inhibitory effects in all stimulation dipoles. In two patients (#1 and #10) we observed a change in polarity of the effect from inhibitory to facilitatory moving the stimulating electrode ventrally and rostrally.

The quantitative analysis on the spatial distribution of inhibitory and facilitatory electrodes yielded 3 principal components, explaining 82%, 14% and 4% of variance respectively. Hotelling's T2 test performed on the first 2 PCs showed that the spatial separation of the two clusters (inhibitory and facilitatory) was highly significant ($T2 = 45.6$, $p = 0.0000003$). The single electrode that showed both facilitatory and inhibitory effects (marked in green in Fig. 4 – right panel) was excluded front he analysis because it could not be classified in any of the two clusters. The results of the cluster analysis are shown in Fig. 4 – right panel. The pattern of inhibition in the dorsal region and excitation in the ventral region was preserved in both hemispheres. Though this resulted in small samples, we looked at patients with right-sided lesions ($n = 8$) and patients with left-sided lesions ($n = 9$) and we found symmetrical results (Supplementary results). However, the small number of patients does not allow for conclusive statements on the lateralization of our observations.

All spots showed the same polarity of effect, whenever present, at all ISIs, with the sole exception of a single spot in a single patient (#3), localized in the intraparietal region, that showed facilitatory effects at the 4 ms ISI and inhibitory effects at the 12 ms ISI. To assess whether the variability of the ISI at which an effect was observed could be related to the distance between test and conditioning electrodes, we ran a correlation analysis. The Euclidean distance between the conditioning and test electrodes (Table 2) that had a significant interaction was correlated with the earliest ISI at which such interaction occurred by means of Spearman's r statistics. The results showed a significant positive correlation ($r = 0.646$, $p = 0.002$), indicating that the longer the distance between pairs of electrodes, the longer was the ISI at which an effect could be observed.

Discussion

Two distinct regions in the parietal cortex exert specific short-latency effects on upper-limb corticospinal excitability

In the present work we demonstrate for the first time the existence of direct parietal-motor functional connections in humans by means of direct cortical stimulation. The presence of short-latency modulations of conditioning stimuli implies that the two regions are functionally connected [40]. This interpretation is corroborated by the significant correlation between inter-electrode distance and the time required for the interactions between the two electrodes to occur (Fig. 6). We identified several cortical spots in the posterior parietal cortex that exert a short-latency effect on the excitability of the corticospinal pathway to the upper limb. Combining spatial distribution and polarity (excitatory or inhibitory) of the conditioning effects, we identified 2 distinct regions: a ventral region, corresponding to the part of the supramarginal gyrus immediately posterior to the inferior postcentral sulcus, extending ventrally to the parietal opercular region, where excitatory effects are clustered and a dorsal region comprising in the superior parietal lobule adjacent to the postcentral sulcus, where inhibitory effects cluster (Fig. 4 left panel). The two clusters are significantly separated in space (Fig. 4 right panel). This main result should be considered in the light of several limitations of the spatial sampling procedure employed here suffers from a main limitation, that is, conditioning stimuli have been delivered on the crown of the sulci, because the surgical procedures do not imply the opening of the arachnoid and widening of the sulci. As such, our map of the parietal cortex is patchy and strongly biased towards the crown of

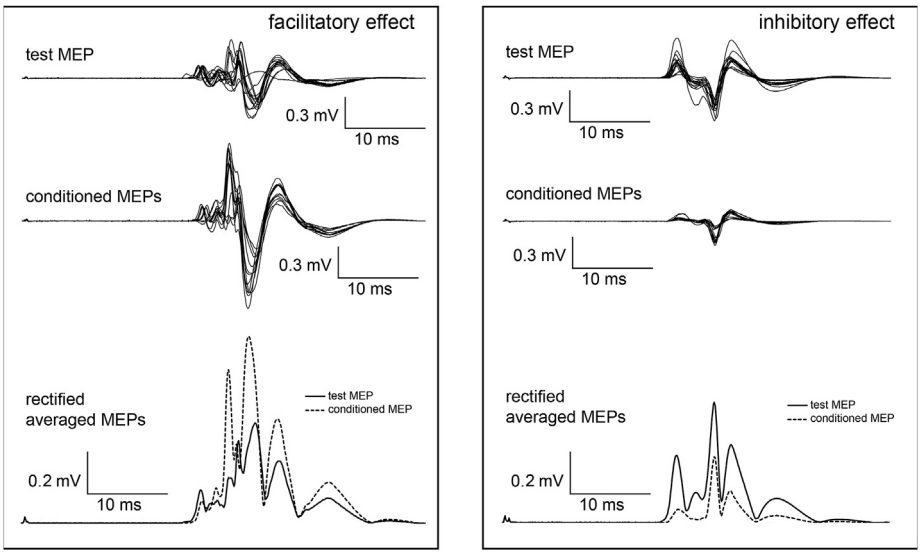

Figure 3. Representative examples of MEP recordings. All EMG recordings are aligned to the last stimulus in the train of test stimulation. In both panels, the upper traces represent 15 superimposed recordings of MEPs produced by test stimuli alone. The middle traces represent conditioned MEPs acquired in an adjacent block. The lower traces represent the average rectified EMG traces obtained from the recordings in the upper and middle traces. The left panel shows an example of facilitatory effects and the left panel shows an example of inhibitory effects of conditioning stimuli on MEP area.

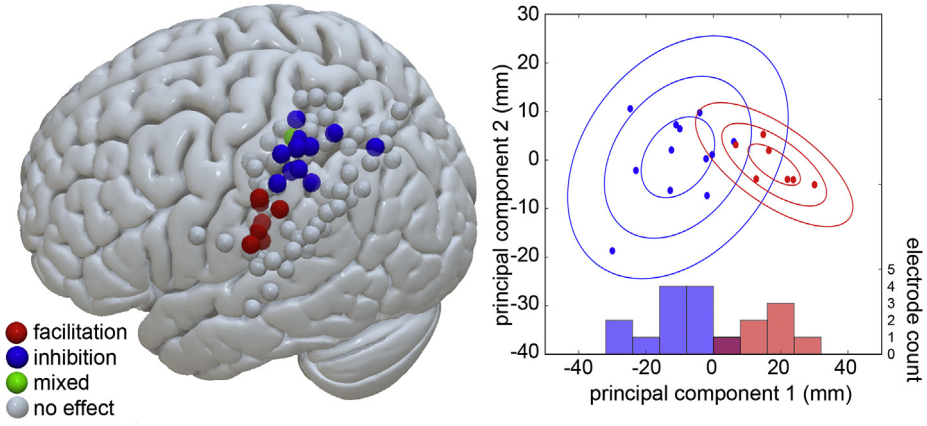

Fig. 4. Left panel: Brain surface template in MNI space on which all the conditioning electrodes (cathodes of the bipolar stimulation setup) have been plotted as spheres of 5 mm in diameter. Electrodes on the central sulcus have been omitted (see text). Grey-filled spheres indicate spots with no significant effect. Blue-filled spheres indicate spots with significant inhibitory conditioning effects. Red-filled spheres indicate spots with significant excitatory conditioning effects. The single electrode in which both excitatory and inhibitory effects were observed at different ISIs is indicated in green. **Right panel:** Coordinates of all electrodes with active effects projected on their first two principal components (PCs). Color coding same as left panel. The first two PCs explain 96% of the variance. The radii of the confidence ellipses are 1, 2 and 3 standard deviations, for each of the two groups. The histogram at the bottom shows the distribution of the coordinates on the 1st principal component. (For interpretation of the references to colour in this figure legend, the reader is referred to the Web version of this article.)

the gyri. We could not therefore sample the banks of the intraparietal sulcus, which is a key region in upper limb motor control [2]. The number of patients studied here is small, and the number of spots sampled per patient is small, being limited by the number of leads in a single strip. However, we should bear in mind that the spatial resolution of bipolar stimulation with electrodes that are 1 cm apart is large (around 1 cm) and, more importantly, each spot is not the result of a single stimulation, but has been tested with a significant number of repeated measures and tested statistically. Each parietal spot represents therefore a stand-alone data point, albeit referred to a single patient. A further caveat in the present brain mapping procedure that is common to most neurosurgical brain maps, is that the population map stems from pooling together all stimulation sites, even if these are not independent samples, given that data from the same strip derives from the same patient. Despite these limitations, the presentation of single-patient data on the cortical map clearly shows that the two cortical regions with active spots represent are “patient-invariant”, i.e. they are not dependent from patient identity. Finally, it should be stressed that, given the exploratory nature of the present study and given the heavy temporal constraint given by surgical procedures, we faced a tradeoff between spatial sampling and temporal sampling. Given the aims of the study, whenever time was limited we decided to test less time intervals (ISIs) and more cortical spots.

Widespread representation of upper limb movements in the posterior parietal cortex

In our study we focussed on the motor representation of the distal upper limb. A striking result is that the posterior parietal

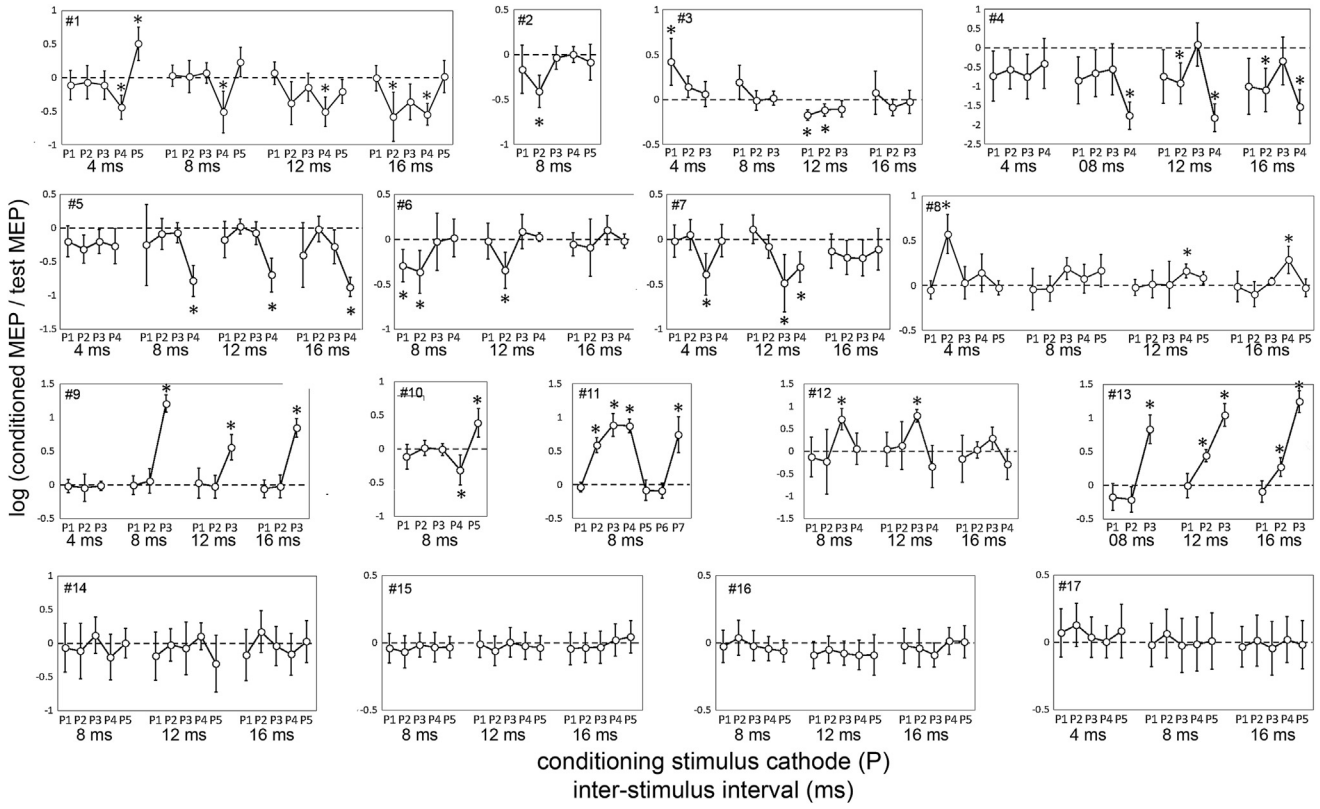

Fig. 5. Comprehensive data from all patients. Each box shows data from one patient indicated in the upper left corner as "#n". Within each box, each graph indicates the data from a given inter-stimulus interval, which is indicated below the x-axis, in milliseconds (ms). Points on the x-axis indicate the single electrodes on the conditioning stimulus strip and correspond to the electrode numbering of Fig. 2. The x-axis of each graph represents therefore a spatially-oriented vector along the conditioning strip. The y axis values indicate the mean log-transformed ratios between conditioned and unconditioned MEPs. Negative values indicate that the mean conditioned MEP is smaller than the mean test MEP (inhibitory effects). Positive values indicate that mean conditioned MEPs are larger than mean test MEPs (excitatory effects). All values have been tested by single-sample t-tests against a null hypothesis of mean value = 0. Significance threshold was Bonferroni corrected in single subjects. Asterisks indicate significant comparisons. Error bars indicate 95% confidence intervals of the mean.

cortex seems to contain a widespread representation of the upper limb. Having tested only one effector, we cannot draw any conclusions on somatotopy, but our partial results argue against a possible somatotopic arrangement of motor representations in the PPC, in opposition of what we could have expected in the premotor region where rough somatotopy is suggested by several studies [58]. Conversely, the posterior parietal cortex, albeit embedded with consistent motor representations, has not been shown to be organized effector-wise in humans. Action representations in the PPC of humans seem to show an upper limb preference and a spatial organization that reflects the type of action rather than the effector used, except for eye movements that are supported by a specialized network [59]. Most authors seem to agree on a motor map of the rostral PPC organized in a medial-lateral system. Spatially-oriented stimuli are coded in the SPL, object-directed movements in the mid-portion, corresponding to the intraparietal sulcus and more complex hand actions such as symbolic movements and tool use are coded in the IPL [2,12]. Consequently, the finding of hand representations throughout its medio-lateral extension is supported by current knowledge on the physiology of motor properties of the human PPC.

A direct parieto-motor pathway in humans

Neuroimaging studies in humans however, are not able to specify the actual neural pathways by which the PPC can modulate movement. The novelty of the present study is providing compelling evidence that one possible neural substrate of the PPC influence on action is fast, probably direct, parieto-motor connectivity. The temporal characteristics of the parieto-motor interactions were not in the focus of the present work because, as stated earlier we sacrificed accuracy in the time course of PPC-M1 interactions in favour of more extensive spatial sampling. We show a general pattern of active spots modulating the output of hand-M1 at ISIs that are roughly proportional to the distance between the active spot and M1, compatibly with axonal conduction of action potentials. Active spots that exert modulation at 4 ms ISIs are all clustered nearby the hand-M1. Active spots that are effective at longer ISIs are located progressively further away from the hand-M1 (Fig. 6). This pattern indicates that effective ISIs scale positively with linear distance to hand-M1. There are two main inferences to be made from this finding: First, that the effect on conditioning stimuli on the PPC is not likely to be due to current spread to M1, because current spread is *quasi*-instantaneous, and the latency of its effect would not increase with distance. Second, the increasing latency of the conditioning effects with increasing distance from M1 argues against the possibility that the site of interaction between parietal output and the corticospinal pathway is subcortical or spinal because in that case we would expect similar latencies of conditioning effects. On the contrary, the pattern of covariation of distance to hand-M1 with effective ISI is strongly in favour of cortico-cortical connections between PPC and hand-M1 mediating the conditioning effect.

Table 3

Statistics on individual patients, for each conditioning electrode and each ISI. The data reported correspond to the log of the ratio between conditioned MEPs and test MEPs. The table reports the mean value (standard deviation), and the t-statistics of the single-sample t-tests: t-value (degrees of freedom) and p-value. Please note that the log-ratio has no dimensions because it is obtained by dividing two identical dimensions. Note also that degrees of freedom are variable according to the number of single trials that were performed in that particular condition. Conditions with p-values exceeding the Bonferroni-corrected significance threshold are highlighted in bold. A graphical representation of the data is provided in Fig. 5.

patient	ISI:	conditioning stimulus cathode				
		P1	P2	P3	P4	P5
#1	4 ms	−0.113 (sd: 0.22) t(19) = -1.17 p = 0.2582	−0.069 (sd: 0.25) t(19) = -0.63 p = 0.5378	−0.112 (sd: 0.21) t(19) = -1.18 p = 0.2544	**−0.441 (sd: 0.18) t(19)=-5.62 p < 0.00001**	**0.508 (sd: 0.25) t(19)=4.59 p=0.0002**
	8 ms	0.03 (sd: 0.16) t(19) = 0.42 p = 0.6856	0.016 (sd: 0.24) t(19) = 0.15 p = 0.8814	0.071 (sd: 0.15) t(19) = 1.08 p = 0.2949	**−0.513 (sd: 0.31) t(19)=-3.69 p=0.0016**	0.232 (sd: 0.22) t(19) = 2.36 p = 0.0288
	12 ms	0.068 (sd: 0.17) t(19) = 0.92 p = 0.3688	−0.38 (sd: 0.32) t(19) = -2.66 p = 0.0156	−0.143 (sd: 0.21) t(19) = -1.54 p = 0.1407	**−0.511 (sd: 0.22) t(19)=-5.16 p=0.0001**	−0.209 (sd: 0.18) t(19) = -2.53 p = 0.0201
	16 ms	−0.005 (sd: 0.19) t(19) = -0.06 p = 0.9584	**−0.585 (sd: 0.37) t(19)=-3.51 p=0.0023**	−0.362 (sd: 0.27) t(19) = -2.98 p = 0.0077	**−0.549 (sd: 0.16) t(19)=-7.81 p < 0.00001**	0.016 (sd: 0.24) t(19) = 0.15 p = 0.8814
#2	8 ms	−0.164 (sd: 0.27) t(14) = -1.39 p = 0.19	**−0.408 (sd: 0.18) t(14)=-5.02 p=0.0002**	−0.035 (sd: 0.13) t(14) = -0.6 p = 0.57	0.002 (sd: 0.09) t(14) = 0.05 p = 0.96	−0.084 (sd: 0.2) t(14) = -0.93 p = 0.37
#3	4 ms	**0.421 (sd: 0.26) t(14)=3.59 p=0.003**	0.142 (sd: 0.12) t(14) = 2.68 p = 0.018	0.062 (sd: 0.14) t(14) = 0.96 p = 0.35		
	8 ms	0.193 (sd: 0.19) t(14) = 2.32 p = 0.03	−0.01 (sd: 0.11) t(14) = -0.2 p = 0.84	0.015 (sd: 0.08) t(14) = 0.44 p = 0.66		
	12 ms	**−0.172 (sd: 0.06) t(14)=-6.26 p < 0.00001**	**−0.115 (sd: 0.07) t(14)=-3.77 p=0.002**	−0.104 (sd: 0.09) t(14) = -2.57 p = 0.02		
	16 ms	0.077 (sd: 0.24) t(14) = 0.72 p = 0.48	−0.087 (sd: 0.09) t(14) = -2.13 p = 0.05	−0.023 (sd: 0.13) t(14) = -0.41 p = 0.69		
#4	4 ms	−0.732 (sd: 0.56) t(14) = -2.53 p = 0.02	−0.56 (sd: 0.44) t(14) = -2.45 p = 0.028	−0.747 (sd: 0.5) t(14) = -2.88 p = 0.01	−0.407 (sd: 0.56) t(14) = -1.41 p = 0.18	
	8 ms	−0.85 (sd: 0.53) t(14) = -3.12 p = 0.008	−0.653 (sd: 0.53) t(14) = -2.38 p = 0.032	−0.556 (sd: 0.57) t(14) = -1.9 p = 0.078	**−1.762 (sd: 0.3) t(14)=-11.33 p < 0.00001**	
	12 ms	−0.744 (sd: 0.6) t(14) = -2.4 p = 0.03	−0.92 (sd: 0.46) t(14) = -3.88 p = 0.002	0.09 (sd: 0.49) t(14) = 0.36 p = 0.73	**−1.821 (sd: 0.31) t(14)=-11.27 p < 0.00001**	
	16 ms	−1.001 (sd: 0.63) t(14) = -3.09 p = 0.008	**−1.093 (sd: 0.49) t(14)=-4.36 p=0.0007**	−0.334 (sd: 0.54) t(14) = -1.21 p = 0.25	**−1.529 (sd: 0.38) t(14)=-7.81 p < 0.00001**	
#5	4 ms	−0.201 (sd: 0.23) t(19) = -1.92 p = 0.069	−0.313 (sd: 0.21) t(19) = -3.29 p = 0.0038	−0.2 (sd: 0.18) t(19) = -2.43 p = 0.02	−0.269 (sd: 0.26) t(19) = -2.34 p = 0.03	
	8 ms	−0.251 (sd: 0.6) t(19) = -0.93 p = 0.36	−0.087 (sd: 0.23) t(19) = -0.83 p = 0.41	−0.07 (sd: 0.15) t(19) = -1.02 p = 0.32	**−0.783 (sd: 0.23) t(19)=-7.75 p < 0.00001**	
	12 ms	−0.173 (sd: 0.27) t(19) = -1.43 p = 0.16	0.023 (sd: 0.11) t(19) = 0.47 p = 0.65	−0.076 (sd: 0.17) t(19) = -1.01 p = 0.33	**−0.696 (sd: 0.25) t(19)=-6.23 p < 0.00001**	
	16 ms	−0.403 (sd: 0.48) t(19) = -1.88 p = 0.07	−0.018 (sd: 0.19) t(19) = -0.21 p = 0.83	−0.276 (sd: 0.25) t(19) = -2.51 p = 0.022	**−0.874 (sd: 0.14) t(19)=-13.62 p < 0.00001**	
#6	8 ms	**−0.291 (sd: 0.18) t(12)=-3.59 p=0.004**	−0.362 (sd: 0.24) t(12) = -3.36 p = 0.006	−0.027 (sd: 0.32) t(12) = -0.19 p = 0.86	0.016 (sd: 0.21) t(12) = 0.17 p = 0.87	
	12 ms	−0.018 (sd: 0.2) t(12) = -0.2 p = 0.84	**−0.343 (sd: 0.2) t(12)=-3.79 p=0.0026**	0.086 (sd: 0.19) t(12) = 1.02 p = 0.33	0.026 (sd: 0.05) t(12) = 1.13 p = 0.29	
	16 ms	−0.054 (sd: 0.13) t(12) = -0.93 p = 0.37	−0.093 (sd: 0.32) t(12) = -0.65 p = 0.53	0.104 (sd: 0.16) t(12) = 1.48 p = 0.17	−0.019 (sd: 0.08) t(12) = -0.52 p = 0.61	
#7	4 ms	−0.02 (sd: 0.18) t(15) = -0.25 p = 0.80	0.049 (sd: 0.17) t(15) = 0.65 p = 0.52	**−0.388 (sd: 0.23) t(15)=-3.71 p=0.002**	−0.015 (sd: 0.18) t(15) = -0.19 p = 0.85	
	8 ms	0.113 (sd: 0.16) t(15) = 1.55 p = 0.14	−0.081 (sd: 0.13) t(15) = -1.36 p = 0.20	−0.488 (sd: 0.32) t(15) = -3.42 p = 0.004	**−0.309 (sd: 0.17) t(15)=-4.1 p=0.0009**	
	16 ms	−0.132 (sd: 0.19) t(15) = -1.55 p = 0.14	−0.203 (sd: 0.19) t(15) = -2.44 p = 0.03	−0.209 (sd: 0.2) t(15) = -2.39 p = 0.030	−0.111 (sd: 0.23) t(15) = -1.1 p = 0.29	
#8	4 ms	−0.051 (sd: 0.1) t(14) = -1.16 p = 0.27	**0.573 (sd: 0.22) t(14)=5.72 p=0.0001**	0.027 (sd: 0.18) t(14) = 0.34 p = 0.74	0.141 (sd: 0.21) t(14) = 1.47 p = 0.16	−0.027 (sd: 0.08) t(14) = -0.74 p = 0.48
	8 ms	−0.043 (sd: 0.23) t(14) = -0.43 p = 0.67	−0.039 (sd: 0.14) t(14) = -0.65 p = 0.53	0.188 (sd: 0.12) t(14) = 3.37 p = 0.004	0.076 (sd: 0.16) t(14) = 1.05 p = 0.31	0.165 (sd: 0.18) t(14) = 2.05 p = 0.06
	12 ms					

(*continued on next page*)

Table 3 (*continued*)

patient	ISI:	conditioning stimulus cathode				
		P1	P2	P3	P4	P5
		−0.022 (sd: 0.09) t(14) = -0.54 p = 0.60	0.016 (sd: 0.15) t(14) = 0.23 p = 0.82	0.007 (sd: 0.26) t(14) = 0.06 p = 0.95	**0.16 (sd: 0.08) t(14)=4.49 p=0.0005**	0.084 (sd: 0.07) t(14) = 2.54 p = 0.02
	16 ms	−0.012 (sd: 0.17) t(14) = -0.15 p = 0.88	−0.099 (sd: 0.14) t(14) = -1.6 p = 0.13	0.046 (sd: 0.04) t(14) = 2.93 p = 0.012	**0.285 (sd: 0.15) t(14)=4.21 p=0.0009**	−0.026 (sd: 0.1) t(14) = -0.57 p = 0.58
#9	4 ms	−0.018 (sd: 0.1) t(22) = -0.39 p = 0.70	−0.042 (sd: 0.2) t(22) = -0.46 p = 0.65	−0.014 (sd: 0.07) t(22) = -0.47 p = 0.65		
	8 ms	−0.006 (sd: 0.14) t(22) = -0.09 p = 0.93	0.059 (sd: 0.18) t(22) = 0.72 p = 0.48	**1.208 (sd: 0.13) t(22)=20.46 p < 0.00001**		
	12 ms	0.026 (sd: 0.22) t(22) = 0.26 p = 0.7932	−0.026 (sd: 0.17) t(22) = -0.34 p = 0.73	**0.558 (sd: 0.19) t(22)=6.62 p < 0.00001**		
	16 ms	−0.057 (sd: 0.13) t(22) = -0.95 p = 0.35	−0.023 (sd: 0.17) t(22) = -0.3 p = 0.77	**0.845 (sd: 0.14) t(22)=13.17 p < 0.00001**		
#10	8 ms	−0.116 (sd: 0.18) t(13) = -1.46 p = 0.1676	0.016 (sd: 0.11) t(13) = 0.33 p = 0.7491	−0.007 (sd: 0.09) t(13) = -0.17 p = 0.8681	**−0.312 (sd: 0.22) t(13)=-3.17 p=0.0075**	**0.387 (sd: 0.21) t(13)=4.12 p=0.0012**
#11	8 ms	**0.885 (sd: 0.17) t(13)=11.58 p < 0.00001**	**0.871 (sd: 0.1) t(13)=19.65 p < 0.00001**	−0.085 (sd: 0.15) t(13) = -1.3 p = 0.22	−0.091 (sd: 0.11) t(13) = -1.87 p = 0.084	**0.74 (sd: 0.27) t(13)=6.09 p < 0.00001**
#12	8 ms	−0.131 (sd: 0.44) t(15) = -0.67 p = 0.51	−0.231 (sd: 0.72) t(15) = -0.72 p = 0.49	**0.715 (sd: 0.24) t(15)=6.81 p < 0.00001**	0.058 (sd: 0.35) t(15) = 0.37 p = 0.71	
	12 ms	0.041 (sd: 0.38) t(15) = 0.24 p = 0.81	0.122 (sd: 0.53) t(15) = 0.52 p = 0.61	**0.791 (sd: 0.14) t(15)=12.91 p < 0.00001**	−0.343 (sd: 0.47) t(15) = -1.64 p = 0.12	
	16 ms	−0.167 (sd: 0.52) t(15) = -0.72 p = 0.48	0.03 (sd: 0.18) t(15) = 0.37 p = 0.71	0.288 (sd: 0.25) t(15) = 2.56 p = 0.02	−0.288 (sd: 0.34) t(15) = -1.9 p = 0.08	
#13	8 ms	−0.174 (sd: 0.2) t(14) = -1.92 p = 0.07	−0.211 (sd: 0.19) t(14) = -2.46 p = 0.03	**0.833 (sd: 0.21) t(14)=8.93 p < 0.00001**		
	12 ms	−0.005 (sd: 0.18) t(14) = -0.06 p = 0.95	**0.441 (sd: 0.09) t(14)=10.64 p < 0.00001**	**1.044 (sd: 0.17) t(14)=14.06 p < 0.00001**		
	16 ms	−0.093 (sd: 0.16) t(14) = -1.29 p = 0.22	**0.274 (sd: 0.14) t(14)=4.54 p=0.0005**	**1.242 (sd: 0.16) t(14)=17.91 p < 0.00001**		
#14	8 ms	−0.039 (sd: 0.11) t(13) = -0.81 p = 0.43	−0.068 (sd: 0.12) t(13) = -1.29 p = 0.22	−0.015 (sd: 0.09) t(13) = -0.37 p = 0.72	−0.034 (sd: 0.11) t(13) = -0.7 p = 0.49	−0.032 (sd: 0.08) t(13) = -0.91 p = 0.38
	12 ms	−0.009 (sd: 0.1) t(13) = -0.2 p = 0.85	−0.061 (sd: 0.11) t(13) = -1.24 p = 0.24	0.004 (sd: 0.11) t(13) = 0.08 p = 0.94	−0.023 (sd: 0.1) t(13) = -0.53 p = 0.61	−0.035 (sd: 0.09) t(13) = -0.87 p = 0.40
	16 ms	−0.043 (sd: 0.12) t(-1) = -0.81 p = 0.43	−0.036 (sd: 0.11) t(13) = -0.73 p = 0.48	−0.032 (sd: 0.12) t(13) = -0.6 p = 0.56	0.02 (sd: 0.12) t(13) = 0.39 p = 0.71	0.046 (sd: 0.12) t(13) = 0.87 p = 0.40
#15	8 ms	−0.026 (sd: 0.12) t(13) = -0.48 p = 0.64	0.037 (sd: 0.13) t(13) = 0.63 p = 0.54	−0.021 (sd: 0.11) t(13) = -0.43 p = 0.67	−0.043 (sd: 0.09) t(13) = -1.12 p = 0.28	−0.061 (sd: 0.08) t(13) = -1.74 p = 0.11
	12 ms	−0.091 (sd: 0.1) t(13) = -2.07 p = 0.06	−0.049 (sd: 0.1) t(13) = -1.06 p = 0.31	−0.077 (sd: 0.09) t(13) = -1.86 p = 0.09	−0.091 (sd: 0.11) t(13) = -1.85 p = 0.08	−0.089 (sd: 0.15) t(13) = -1.37 p = 0.20
	16 ms	−0.021 (sd: 0.13) t(-1) = -0.37 p = 0.72	−0.038 (sd: 0.14) t(13) = -0.59 p = 0.56	−0.09 (sd: 0.09) t(13) = -2.13 p = 0.05	0.015 (sd: 0.1) t(13) = 0.35 p = 0.72	0.008 (sd: 0.12) t(13) = 0.15 p = 0.89
#16	8 ms	0.071 (sd: 0.18) t(17) = 0.9 p = 0.38	0.13 (sd: 0.16) t(17) = 1.88 p = 0.07	0.038 (sd: 0.15) t(17) = 0.57 p = 0.58	0.005 (sd: 0.12) t(17) = 0.1 p = 0.93	0.084 (sd: 0.2) t(17) = 0.94 p = 0.36
	12 ms	−0.018 (sd: 0.16) t(17) = -0.26 p = 0.80	0.065 (sd: 0.18) t(17) = 0.82 p = 0.42	−0.022 (sd: 0.2) t(17) = -0.25 p = 0.80	−0.013 (sd: 0.2) t(17) = -0.15 p = 0.88	0.01 (sd: 0.21) t(17) = 0.11 p = 0.91
	16 ms	−0.034 (sd: 0.15) t(-1) = -0.51 p = 0.61	0.013 (sd: 0.19) t(17) = 0.15 p = 0.88	−0.044 (sd: 0.2) t(17) = -0.49 p = 0.63	0.021 (sd: 0.17) t(17) = 0.28 p = 0.78	−0.017 (sd: 0.18) t(17) = -0.22 p = 0.83
#17	4 ms	−0.066 (sd: 0.36) t(13) = -0.42 p = 0.68	−0.116 (sd: 0.41) t(13) = -0.64 p = 0.53	0.118 (sd: 0.27) t(13) = 0.97 p = 0.35	−0.205 (sd: 0.34) t(13) = -1.37 p = 0.19	0.002 (sd: 0.22) t(13) = 0.02 p = 0.98
	8 ms	−0.189 (sd: 0.36) t(13) = -1.18 p = 0.26	−0.022 (sd: 0.24) t(13) = -0.2 p = 0.85	−0.074 (sd: 0.39) t(13) = -0.43 p = 0.67	0.106 (sd: 0.2) t(13) = 1.18 p = 0.26	−0.302 (sd: 0.42) t(13) = -1.61 p = 0.13
	16 ms	−0.173 (sd: 0.38) t(13) = -1.03 p = 0.32	0.174 (sd: 0.31) t(13) = 1.28 p = 0.22	−0.04 (sd: 0.29) t(13) = -0.3 p = 0.77	−0.163 (sd: 0.31) t(13) = -1.18 p = 0.26	0.026 (sd: 0.31) t(13) = 0.19 p = 0.85

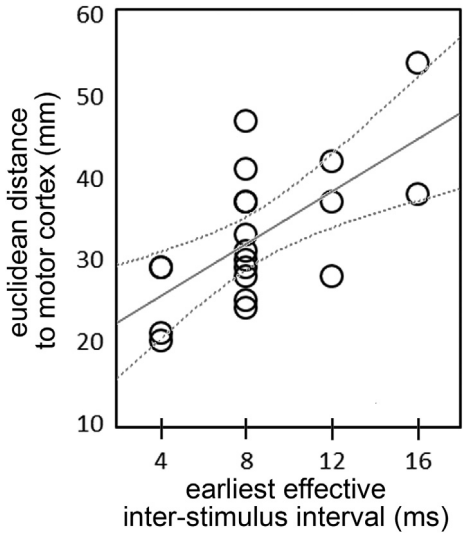

Fig. 6. Scatterplot of the surface (Euclidean) distance between all pairs of conditioning and test electrodes at which a significant effect has been observed and the earliest ISI at which such effect has become evident. Each circle represents a single pair of conditioning-test electrodes. The continuous line represents the correlation line according to Spearman's r test. The dashed lines indicate upper and lower 95% confidence intervals of the correlation line. Spearman's test showed a significant positive correlation ($r = 0.646$, $p = 0.002$).

Effects of anaesthesia

All our patients have been tested under the TIVA protocol. The main effect of propofol is a strong enhancement of GABAergic inputs [60]. In terms of brain connectivity, Propofol dampens extensive cortico-cortical connections, according to TMS-EEG studies [61]. The strength of oligosynaptic pathways is affected but generally not to the level of a conduction block, as witnessed by the validity of somatosensory evoked potentials and motor evoked potentials, which are mediated by multi-synaptic neural chains. The TIVA protocol is titrable, and it was systematically kept at low levels of neural suppression (see methods). Therefore, the anaesthesiologic setting employed here is appropriate to test mono- or oligo-synaptic connections, though we cannot make any inference on how these connections would work in the awake state. Summing up, the implications of testing cortico-cortical connectivity under anaesthesia are that: A) significant effects can be considered as genuine expression of oligo-synaptic connections, B) non-significant stimulations could underlie either no connections or multi-synaptic connections which are dampened by anaesthesia and C) we cannot make any inference on how the highlighted connections would function in the awake state and even more so during active tasks.

Relation to connectivity data obtained with non-invasive brain stimulation

Ipsilateral PPC-M1 connections have been tested non-invasively by dual-coil TMS in awake subjects in a series of studies [33–41,52,62–65]. The present results cannot be compared to these studies in alert subjects in terms of polarity (inhibition or excitation) nor of task-dependency of the response because of the anaesthesia, but they can be compared in terms of cortical site in the PPC and timing of conditioning stimuli that exert a significant effect onto M1. Our data are compatible with the findings of Karabanov et al. [33] showing two foci along the intraparietal sulcus. The spots nearest to the anterior intraparietal region (Fig. 4) shows striking similarities with the findings of Vesia et al. [52]. The most ventral spots along the postcentral sulcus are in the same location as the opercular region that was stimulated in Maule et al. [39]. The posterior intraparietal spot stimulated in Koch et al. [34,36] is similar or slightly posterior to the most posterior inhibitory spots observed here. Summing up, the current systematic mapping of the PPC is consistent with most of the previous data testing single cortical spots with non-invasive brain stimulation. On the contrary, our data are difficult to match to the existing literature on awake subjects in terms of net polarity of the effect because this is known to be volatile, depending on the task dynamics [36,52] Other authors find different properties of PPC organized in a caudal-rostral direction. Karabanov [33] found that along the lower lip off the IPS, anterior spots had an inhibitory effect and posterior spots had a facilitatory effect. Finally, a recent paper by Brown et al. [66] shows that TMS of the postcentral region very near to the superior parietal targets described in the present work, elicits inhibitory short-latency effects on the ipsilateral M1.

Conclusion

We show conclusive evidence that in humans direct parieto-motor pathways exist. We investigated motor output to the distal upper limb and found a widespread representation of the hand with seemingly no specific spatial distribution that could parallel the somatotopy of the adjacent somatosensory cortex. Such absence of topographic distribution is well supported by previous data in non-human and human primates that indicate a spatial organization of motor features in the PPC reflecting action types rather than effectors. We did find a specific spatial clustering of motor spots in the PPC according to the polarity of the effect on corticospinal output and to spatial location. A ventral cluster showed excitatory effects, while a dorsal cluster showed inhibitory effects. Though the clinical neurosurgeon's attention toward motor function of the parietal lobe is increasingly recognized [67], in the present data we do not show any correlation of parietal-M1 connectivity do specific behavioural patterns, and therefore the present data have no direct clinical meaning. Nevertheless, the present work shows for the first time the possibility to explore brain connectivity in the asleep patient during neurosurgery. The dual-coil stimulation technique is potentially suitable to assess any other cortico-cortical connection in the human brain.

Funding

PM has been supported by the Brain Research Foundation of Verona (https://www.brainresearchfoundationverona.org/).

Declaration of competing interest

The authors report no competing interests.

CRediT authorship contribution statement

Luigi Cattaneo: Conceptualization, Methodology, Formal analysis, Investigation, Writing - original draft, Visualization, Supervision. **Davide Giampiccolo:** Methodology, Formal analysis, Investigation, Writing - original draft, Visualization. **Pietro Meneghelli:** Methodology, Formal analysis, Investigation, Writing - original draft, Visualization. **Vincenzo Tramontano:** Methodology, Investigation, Data curation. **Francesco Sala:** Methodology, Investigation, Writing - original draft, Resources, Project administration, Funding acquisition, Supervision.

Acknowledgements

we wish to acknowledge Emanuele Olivetti for the considerable help in data analysis and Federica Basaldella, Dr. Francesco Cozzi, Dr. Fabio Moscolo and Dr. Angelo Musumeci for the valuable help in data collection.

Appendix A. Supplementary data

Supplementary data to this article can be found online at https://doi.org/10.1016/j.brs.2020.02.023.

References

[1] Mountcastle VB, Lynch JC, Georgopoulos AP, Sakata H, Acuna C. Posterior parietal association cortex of the monkey: command functions for operations within extrapersonal space. J Neurophysiol 1975;38:871–908.
[2] Orban GA. Functional definitions of parietal areas in human and non-human primates. Proc R Soc B Biol Sci 2016;283. https://doi.org/10.1098/rspb.2016.0118. 20160118.
[3] Jeannerod M. The hand and the object: the role of posterior parietal cortex in forming motor representations. Can J Physiol Pharemacology 1994;72:535–41.
[4] Buxbaum LJ, Randerath J. Limb apraxia and the left parietal lobe. Handb Clin Neurol 2018. https://doi.org/10.1016/B978-0-444-63622-5.00017-6.
[5] Turella L, Rumiati R, Lingnau A. Hierarchical action encoding within the human brain. Cerebr Cortex 2019:1–15. https://doi.org/10.1093/cercor/bhz284.
[6] Andersen RA, Andersen KN, Hwang EJ, Hauschild M. Optic ataxia: from balint's syndrome to the parietal reach region. Neuron 2014;81:967–83. https://doi.org/10.1016/j.neuron.2014.02.025.
[7] Goldenberg G. Apraxia and the parietal lobes. Neuropsychologia 2009;47:1449–59. https://doi.org/10.1016/j.neuropsychologia.2008.07.014.
[8] Balestrini S, Francione S, Mai R, Castana L, Casaceli G, Marino D, et al. Multimodal responses induced by cortical stimulation of the parietal lobe: a stereoelectroencephalography study. Brain 2015;138:2596–607. https://doi.org/10.1093/brain/awv187.
[9] Penfield W, Boldrey E. Somatic motor and sensory representation in the cerebral cortex of man as studied by electrical stimulation. Brain 1937;60:389–443. https://doi.org/10.1093/brain/60.4.389.
[10] Culham JC, Valyear KF. Human parietal cortex in action. Curr Opin Neurobiol 2006;16:205–12. https://doi.org/10.1016/j.conb.2006.03.005.
[11] Filimon F. Human cortical control of hand movements: parietofrontal networks for reaching, grasping, and pointing. Neuroscientist 2010;16:388–407. https://doi.org/10.1177/1073858410375468.
[12] Gallivan JP, Culham JC. Neural coding within human brain areas involved in actions. Curr Opin Neurobiol 2015;33:141–9. https://doi.org/10.1016/j.conb.2015.03.012.
[13] Monaco S, Sedda A, Cavina-Pratesi C, Culham JC. Neural correlates of object size and object location during grasping actions. Eur J Neurosci 2015;41:454–65. https://doi.org/10.1111/ejn.12786.
[14] Cavina-Pratesi C, Connolly JD, Monaco S, Figley TD, Milner AD, Schenk T, et al. Human neuroimaging reveals the subcomponents of grasping, reaching and pointing actions. Cortex 2018;98:128–48. https://doi.org/10.1016/j.cortex.2017.05.018.
[15] Culham JC, Danckert SL, DeSouza JFX, Gati JS, Menon RS, Goodale MA. Visually guided grasping produces fMRI activation in dorsal but not ventral stream brain areas. Exp Brain Res 2003;153:180–9. https://doi.org/10.1007/s00221-003-1591-5.
[16] Frey SH, Vinton D, Norlund R, Grafton ST. Cortical topography of human anterior intraparietal cortex active during visually guided grasping. Cognit Brain Res 2005;23:397–405. https://doi.org/10.1016/j.cogbrainres.2004.11.010.
[17] Begliomini C, Wall MB, Smith AT, Castiello U. Differential cortical activity for precision and whole-hand visually guided grasping in humans. Eur J Neurosci 2007;25:1245–52. https://doi.org/10.1111/j.1460-9568.2007.05365.x.
[18] Stark A, Zohary E. Parietal mapping of visuomotor transformations during human tool grasping. Cerebr Cortex 2008;18:2358–68. https://doi.org/10.1093/cercor/bhm260.
[19] Hinkley LBN, Krubitzer LA, Padberg J, Disbrow EA. Visual-manual exploration and posterior parietal cortex in humans. J Neurophysiol 2009;102:3433–46. https://doi.org/10.1152/jn.90785.2008.
[20] Grol MJ, Majdandzic J, Stephan KE, Verhagen L, Dijkerman HC, Bekkering H, et al. Parieto-frontal connectivity during visually guided grasping. J Neurosci 2007;27:11877–87. https://doi.org/10.1523/JNEUROSCI.3923-07.2007.
[21] Verhagen L, Dijkerman HC, Medendorp WP, Toni I. Cortical dynamics of sensorimotor integration during grasp planning. J Neurosci 2012;32:4508–19. https://doi.org/10.1523/JNEUROSCI.5451-11.2012.
[22] Eickhoff SB, Schleicher A, Zilles K, Amunts K. The human parietal operculum. I. Cytoarchitectonic mapping of subdivisions. Cerebr Cortex 2006;16:254–67. https://doi.org/10.1093/cercor/bhi105.
[23] Eickhoff SB, Amunts K, Mohlberg H, Zilles K. The human parietal operculum. II. Stereotaxic maps and correlation with functional imaging results. Cerebr Cortex 2006;16:268–79. https://doi.org/10.1093/cercor/bhi106.
[24] Eickhoff SB, Jbabdi S, Caspers S, Laird a R, Fox PT, Zilles K, et al. Anatomical and functional connectivity of cytoarchitectonic areas within the human parietal operculum. J Neurosci 2010;30:6409–21. https://doi.org/10.1523/JNEUROSCI.5664-09.2010.
[25] Kaas JH, Stepniewska I. Evolution of posterior parietal cortex and parietal-frontal networks for specific actions in primates. J Comp Neurol 2016;524:595–608. https://doi.org/10.1002/cne.23838.
[26] Wise SP, Boussaoud D, Johnson PB, Caminiti R. Premotor and parietal cortex: corticocortical connectivity and combinatorial computations. Annu Rev Neurosci 2002;20:25–42. https://doi.org/10.1146/annurev.neuro.20.1.25.
[27] Murata A, Fadiga L, Fogassi L, Gallese V, Raos V, Rizzolatti G. Object representation in the ventral premotor cortex (area F5) of the monkey. J Neurophysiol 1997;78:2226–30.
[28] Rizzolatti G, Cattaneo L, Fabbri-Destro M, Rozzi S. Cortical mechanisms underlying the organization of goal-directed actions and mirror neuron-based action understanding. Physiol Rev 2014;94:655–706. https://doi.org/10.1152/physrev.00009.2013.
[29] Bruni S, Gerbella M, Bonini L, Borra E, Coudé G, Ferrari PF, et al. Cortical and subcortical connections of parietal and premotor nodes of the monkey hand mirror neuron network. Brain Struct Funct 2018;223:1713–29. https://doi.org/10.1007/s00429-017-1582-0.
[30] Strick PL, Kim CC. Input to primate motor cortex from posterior parietal cortex (area 5). I. Demonstration by retrograde transport. Brain Res 1978;157:325–30. https://doi.org/10.1016/0006-8993(78)90035-5.
[31] Rozzi S, Calzavara R, Belmalih A, Borra E, Gregoriou GG, Matelli M, et al. Cortical connections of the inferior parietal cortical convexity of the macaque monkey. Cerebr Cortex 2006;16:1389–417. https://doi.org/10.1093/cercor/bhj076.
[32] Rathelot JA, Dum RP, Strick PL. Posterior parietal cortex contains a command apparatus for hand movements. Proc Natl Acad Sci U S A 2017;114:4255–60. https://doi.org/10.1073/pnas.1608132114.
[33] Karabanov AN, Chao CC, Paine R, Hallett M. Mapping different intrahemispheric parietal-motor networks using twin coil TMS. Brain Stimul 2013;6:384–9. https://doi.org/10.1016/j.brs.2012.08.002.
[34] Koch G, Del Olmo MF, Cheeran B, Ruge D, Schippling S, Caltagirone C, et al. Focal stimulation of the posterior parietal cortex increases the excitability of the ipsilateral motor cortex. J Neurosci 2007;27:6815–22. https://doi.org/10.1523/JNEUROSCI.0598-07.2007.
[35] Koch G, Cercignani M, Pecchioli C, Versace V, Oliveri M, Caltagirone C, et al. In vivo definition of parieto-motor connections involved in planning of grasping movements. Neuroimage 2010;51:300–12. https://doi.org/10.1016/j.neuroimage.2010.02.022.
[36] Koch G, Del Olmo MF, Cheeran B, Schippling S, Caltagirone C, Driver J, et al. Functional interplay between posterior parietal and ipsilateral motor cortex revealed by twin-coil transcranial magnetic stimulation during reach planning toward contralateral space. J Neurosci 2008;28:5944–53. https://doi.org/10.1523/JNEUROSCI.0957-08.2008.
[37] Ziluk A, Premji A, Nelson AJ. Functional connectivity from area 5 to primary motor cortex via paired-pulse transcranial magnetic stimulation. Neurosci Lett 2010;484:81–5. https://doi.org/10.1016/j.neulet.2010.08.025.
[38] Cattaneo L, Barchiesi G. Transcranial magnetic mapping of the short-latency modulations of corticospinal activity from the ipsilateral hemisphere during rest. Front Neural Circ 2011;5:1–13. https://doi.org/10.3389/fncir.2011.00014.
[39] Maule F, Barchiesi G, Brochier T, Cattaneo L. Haptic working memory for grasping: the role of the parietal operculum. Cerebr Cortex 2015;25:528–37. https://doi.org/10.1093/cercor/bht252.
[40] Koch G, Rothwell JC. TMS investigations into the task-dependent functional interplay between human posterior parietal and motor cortex. Behav Brain Res 2009;202:147–52. https://doi.org/10.1016/j.bbr.2009.03.023.
[41] Vesia M, Davare M. Decoding action intentions in parietofrontal circuits. J Neurosci 2011;31:16491–3. https://doi.org/10.1523/JNEUROSCI.4408-11.2011.
[42] Guye M, Parker GJ, Symms M, Boulby P, Wheeler-Kingshott CA, Salek-Haddadi A, et al. Combined functional MRI and tractography to demonstrate the connectivity of the human primary motor cortex in vivo. Neuroimage 2003;19:1349–60. https://doi.org/10.1016/S1053-8119(03)00165-4.
[43] Yin X, Zhao L, Xu J, Evans AC, Fan L, Ge H, et al. Anatomical substrates of the alerting, orienting and executive control components of attention: focus on the posterior parietal lobe. PloS One 2012;7:e50590. https://doi.org/10.1371/journal.pone.0050590.
[44] Hanajima R, Ashby P, Lang AE, Lozano AM. Effects of acute stimulation through contacts placed on the motor cortex for chronic stimulation. Clin Neurophysiol 2002;113:635–41. https://doi.org/10.1016/S1388-2457(02)00042-1.
[45] Katayama Y, Tsubokawa T, Maejima S, Hirayama T, Yamamoto T. Corticospinal direct response in humans: identification of the motor cortex during intracranial surgery under general anaesthesia. J Neurol Neurosurg Psychiatry 1988;51:50–9. https://doi.org/10.1136/jnnp.51.1.50.
[46] Lefaucheur JP, Holsheimer J, Goujon C, Keravel Y, Nguyen JP. Descending volleys generated by efficacious epidural motor cortex stimulation in patients

with chronic neuropathic pain. Exp Neurol 2010;223:609–14. https://doi.org/10.1016/j.expneurol.2010.02.008.
[47] Yamamoto T, Katayama Y, Nagaoka T, Kobayashi K, Fukaya C. Intraoperative monitoring of the corticospinal Motor Evoked potential (D-wave): clinical index for Postoperative Motor function and functional recovery. Neurol Med -Chir 2004;44:170–82.
[48] Hardwick RM, Caspers S, Eickhoff SB, Swinnen SP. Neural correlates of action: comparing meta-analyses of imagery, observation, and execution. Neurosci Biobehav Rev 2018. https://doi.org/10.1016/j.neubiorev.2018.08.003.
[49] Shattuck DW, Leahy RM. Brainsuite: an automated cortical surface identification tool. Med Image Anal 2002. https://doi.org/10.1016/S1361-8415(02)00054-3.
[50] Romstöck J, Fahlbusch R, Ganslandt O, Nimsky C, Strauss C. Localisation of the sensorimotor cortex during surgery for brain tumours: feasibility and waveform patterns of somatosensory evoked potentials. J Neurol Neurosurg Psychiatry 2002;72:221–9. https://doi.org/10.1136/jnnp.72.2.221.
[51] Cerri G, Shimazu H, Maier MA, Lemon RN. Facilitation from ventral premotor cortex of primary motor cortex outputs to macaque hand muscles. J Neurophysiol 2003;90:832–42. https://doi.org/10.1152/jn.01026.2002.
[52] Vesia M, Bolton DA, Mochizuki G, Staines WR. Human parietal and primary motor cortical interactions are selectively modulated during the transport and grip formation of goal-directed hand actions. Neuropsychologia 2013;51:410–7. https://doi.org/10.1016/j.neuropsychologia.2012.11.022.
[53] Kiers L, Cros D, Chiappa KH, Fang J. Variability of motor potentials evoked by transcranial magnetic stimulation. Electroencephalogr Clin Neurophysiol Evoked Potentials 1993;89:415–23. https://doi.org/10.1016/0168-5597(93)90115-6.
[54] McDonnell MN, Ridding MC, Miles TS. Do alternate methods of analysing motor evoked potentials give comparable results? J Neurosci Methods 2004. https://doi.org/10.1016/j.jneumeth.2003.12.020.
[55] Groppa S, Oliviero A, Eisen A, Quartarone A, Cohen LG, Mall V, et al. A practical guide to diagnostic transcranial magnetic stimulation: report of an IFCN committee. Clin Neurophysiol 2012;123:858–82. https://doi.org/10.1016/j.clinph.2012.01.010.
[56] Zlatkina V, Petrides M. Morphological patterns of the intraparietal sulcus and the anterior intermediate parietal sulcus of jensen in the human brain. Proc R Soc B Biol Sci 2014;281:1–8. https://doi.org/10.1098/rspb.2014.1493.
[57] Hotelling H. The generalization of student's ratio. Ann Math Stat 1931. https://doi.org/10.1214/aoms/1177732979.
[58] Cunningham DA, Machado A, Yue GH, Carey JR, Plow EB. Functional somatotopy revealed across multiple cortical regions using a model of complex motor task. Brain Res 2013;1531:25–36. https://doi.org/10.1016/j.brainres.2013.07.050.
[59] Grefkes C, Fink GR. The functional organization of the intraparietal sulcus in humans and monkeys. J Anat 2005;207:3–17. https://doi.org/10.1111/j.1469-7580.2005.00426.x.
[60] Franks NP. General anaesthesia: from molecular targets to neuronal pathways of sleep and arousal. Nat Rev Neurosci 2008;9:370–86. https://doi.org/10.1038/nrn2372.
[61] Sarasso S, Boly M, Napolitani M, Gosseries O, Charland-Verville V, Casarotto S, et al. Consciousness and complexity during unresponsiveness induced by propofol, xenon, and ketamine. Curr Biol 2015;25:3099–105. https://doi.org/10.1016/j.cub.2015.10.014.
[62] Vesia M, Barnett-Cowan M, Elahi B, Jegatheeswaran G, Isayama R, Neva JL, et al. Human dorsomedial parieto-motor circuit specifies grasp during the planning of goal-directed hand actions. Cortex 2017;92:175–86. https://doi.org/10.1016/j.cortex.2017.04.007.
[63] Chao CC, Karabanov AN, Paine R, Carolina De Campos A, Kukke SN, Wu T, et al. Induction of motor associative plasticity in the posterior parietal cortex-primary motor network. Cerebr Cortex 2015;25:365–73. https://doi.org/10.1093/cercor/bht230.
[64] Koch G, Oliveri M, Cheeran B, Ruge D, Gerfo E Lo, Salerno S, et al. Hyperexcitability of parietal-motor functional connections in the intact left-hemisphere of patients with neglect. Brain 2008;131:3147–55. https://doi.org/10.1093/brain/awn273.
[65] Karabanov A, Jin SH, Joutsen A, Poston B, Aizen J, Ellenstein A, et al. Timing-dependent modulation of the posterior parietal cortex-primary motor cortex pathway by sensorimotor training. J Neurophysiol 2012;107:3190–9. https://doi.org/10.1152/jn.01049.2011.
[66] Brown MJN, Weissbach A, Pauly MG, Vesia M, Gunraj C, Baarbé J, et al. Somatosensory-motor cortex interactions measured using dual-site transcranial magnetic stimulation. Brain Stimul 2019;12:1229–43. https://doi.org/10.1016/j.brs.2019.04.009.
[67] Rossi M, Fornia L, Puglisi G, Leonetti A, Zuccon G, Fava E, et al. Assessment of the praxis circuit in glioma surgery to reduce the incidence of postoperative and long-term apraxia: a new intraoperative test. J Neurosurg 2018;130:1–11. https://doi.org/10.3171/2017.7.JNS17357.